arXiv:1009.5679v1 [astro-ph.CO] 28 Sep 2010

H I Clouds in the M81 Filament as Dark Matter Minihalos–A Phase-Space Mismatch.

Katie M. Chynoweth
Naval Research Laboratory, Washington, DC 20375

Glen I. Langston
National Radio Astronomy Observatory, Green Bank, WV 24944

Kelly Holley-Bockelmann
Vanderbilt University, Physics and Astronomy Department, 1807 Station B, Nashville, TN 37235

ABSTRACT

Cosmological galaxy formation models predict the existence of dark matter minihalos surrounding galaxies and in filaments connecting groups of galaxies. The more massive of these minihalos are predicted to host H I gas that should be detectable by current radio telescopes such as the GBT. We observed the region including the M81/M82 and NGC 2403 galaxy groups, searching for observational evidence of an H I component associated with dark matter halos within the "M81 Filament", using the Robert C. Byrd Green Bank Telescope (GBT). The map covers an 8.7° × 21.3 ° (480 kpc × 1.2 Mpc) region centered between the M81/M82 and NGC 2403 galaxy groups. Our observations cover a wide velocity range, from -890 to 1320 km s^{-1}, which spans much of the range predicted by cosmological N-body simulations for dark matter minihalo velocities. Our search is not complete in the velocity range -210 to 85 km s^{-1}, containing Galactic emission and the HVC Complex A. For an H I cloud at the distance of M81, with a size $\leq$ 10 kpc, our average 5σ mass detection limit is 3.2 × 10^6 $M_\odot$, for a linewidth of 20 km s^{-1}. We compare our observations to two large cosmological N-body simulations and find that the simulation predicts a significantly greater number of detectable minihalos than are found in our observations, and that the simulated minihalos do not match the phase space of observed H I clouds. These results place strong constraints on the H I gas that can be associated with dark-matter halos. Our observations indicate that the majority of extragalactic H I clouds with a mass greater than 10^6 $M_\odot$ are likely to be generated through cold accretion, or via tidal stripping caused by galaxy interactions.

Subject headings: galaxies: evolution, galaxies: interactions, ISM: clouds, ISM: evolution, radio lines: galaxies, ISM:HI, cosmology:dark matter,

1. Introduction

ΛCDM cosmological models (e.g., Dekel & Silk (1986); Klypin et al. (1999)) for structure formation in the universe predict many compact dark-matter structures, *minihalos*, in the regions near galaxies and galaxy groups. Ricotti (2009) predicts that minihalos may have a late phase of gas accretion, which will be detectable in H I observations. It has been proposed that at least part of the population of neutral hydrogen High Velocity Clouds (HVCs) surrounding the Milky Way may represent these H I -embedded dark matter halos (Blitz et al. 1999; Braun & Burton 1999; Giovanelli et al. 2010). Other possible origins of the HVCs include galactic fountains (Bregman 1980),

tidal stripping from major and satellite galaxy interactions (Putman et al. 2003; Chynoweth et al. 2008), and cold accretion of primordial gas (Kereš & Hernquist 2009). Observations of the north Galactic polar region by the ALFALFA survey may have revealed low H I mass minihalos surrounding the Milky Way (Giovanelli et al. 2010); however, these clouds may also be part of the Magellanic Stream. Searches for H I counterparts to these minihalos within galaxy groups have yielded non-detections or detections that do not match the predicted phase space (e.g. Pisano et al. (2007); Chynoweth et al. (2008, 2009)).

In this paper, we conduct an H I survey of a 8.7° × 21.3 ° region of a nearby complex of galaxies known as the "M81 Filament" (Karachentsev et al. 2002), in an extensive search for H I clouds that may trace in H I a population of $10^8 - 10^{10} M_\odot$ dark matter minihalos (Kravtsov et al. 2004). The M81 Filament includes the M81/M82 and NGC 2403 galaxy groups and the region between them. It is likely that the linearly shaped set of galaxies is contained within a dark-matter filament of the type commonly seen to form in cosmological simulations. The extent of the dark-matter and hot gaseous halos of these two groups is unknown – in fact, the M81/M82 group is sometimes considered to encompass the NGC 2403 group as part of one cluster (Begum et al. 2006; Karachentsev & Kaisin 2007). If this is true, then we may expect to detect pressure-confined clouds that trace cold accretion and H I -laced dark matter halos in between the two groups, as well as galaxy interaction-generated H I clouds near the strongly interacting M81 Group. With wide velocity coverage and high sensitivity over such a large area, this campaign was designed create a census of the more massive H I clouds, which may be counterparts to minihalos or generated by galaxy interactions.

In Section 2, we summarize the observations. In Section 3, we describe the data reduction process. In Section 4, we discuss the interpretation of the data and sensitivity limits. Section 5 describes our detections. In Section 6, we compare our results with numerical simulations. Finally, Section 7 contains discussion, and we draw conclusions and discuss future work. In Appendix A, we present the H I properties of the galaxies in the observed volume.

2. Observations

Observations were carried out with the 100m Robert C. Byrd Green Bank Telescope (GBT) of the NRAO[1] in 40 sessions between June 2003 and August 2009. This includes data taken for previously published observations of the M81/M82 and NGC 2403 galaxy groups; see Chynoweth et al. (2008) and Chynoweth et al. (2009) for details. We combined the 40 observing sessions into a single 8.7° × 21.3 ° map centered at $08^h40^m37.0^s$, 69°17‘16“. Figure 1 shows a layout of the observations.

The filament was observed by moving the telescope in declination and sampling every 3′ with an integration time of 1-3 seconds per sample, depending on the observation session. Strips of constant declination were spaced by 3′. Corresponding maps were made by moving the telescope in right ascension to form a 'basket weave' pattern over the region. Total integration time for the entire map was approximately 187 hours. In Figure 3 it is possible to infer the RMS noise and corresponding mass sensitivity of the map as a function of position.

The GBT spectrometer was used with a bandwith of either 12.5 or 50 MHz, depending on the observation session. The combined bandwidth for the final map is 10.5 MHz, corresponding to a velocity range from -890 to 1320 km s^{-1}. The typical system temperature for each channel of the dual-polarization receiver was $\sim$ 20 K.

Our observations cover a large angular area in order to make a complete study of the H I properties across the entire extent of the filament. The beam size of the GBT in the 21 cm line is 9′, which maps to approximately 10 kpc at the distance of the M81 filament. This is well matched to the angular size of known H I clouds above our mass detection threshold (Thilker et al. 2004; Chynoweth et al. 2008). Predictions for the sizes of dark-matter minihalos range from 3-30 kpc in diameter (Putman & Moore 2002); we may be unable to detect minihalo clouds with a $\leq$ 10 kpc diameter due to beam dilution.

[1]The National Radio Astronomy Observatory (NRAO) is a facility of the National Science Foundation operated under cooperative agreement by Associated Universities, Inc.

3. Data Reduction

The GBT data were reduced in the standard manner using the GBTIDL and AIPS[2] data reduction packages.

In order to match our velocity resolution to the expected linewidths of H I clouds in the group, spectra were smoothed to a channel spacing of 24.4 kHz, corresponding to a velocity resolution of 5.2 km s^{-1}. A reference spectrum for each of the observation sessions was made using an observation of an emission-free region, usually from the edges of the maps. The reference spectrum was then used to perform a (signal-reference)/reference calibration of each pixel. The calibrated spectra were scaled by the system temperature, corrected for atmospheric opacity and GBT efficiency. We adopted the GBT efficiency equation (1) from Langston & Turner (2007) with a zenith atmospheric opacity $\tau_0 = 0.009$. Velocities are in the kinematic LSR velocity frame.

The frequency range observed was relatively free of RFI, with less than 0.2% of all spectra adversely affected. The spectra exhibiting RFI were identified by tabulating the RMS noise level in channels free of neutral hydrogen emission. Spectra that showed high values of RMS noise across many channels were flagged and removed. Observations were gridded using the AIPS task SDIMG, which also averages polarizations. After amplitude calibration and gridding, a 1st-order polynomial was fit to line-free regions of the spectra and subtracted from the gridded spectra using the AIPS task IMLIN. Only the channels in the velocity range -400 to -800 km s^{-1} were used for the fit. This simple baseline fit was extrapolated to the positive velocity range, where galaxies make a baseline fit unreliable. This baseline velocity range for the fit yielded a flat baseline for areas free of strong continuum radio sources, which is true of the majority of the region. The effective angular resolution, determined from maps of 3C286, is $9.15' \pm 0.05'$. To convert to units of flux density, we observed the calibration source 3C286, whose flux density is 14.57 ± 0.94 Jy at 1.418 GHz (Ott et al. 1994). The calibration from K to Jy was derived by mapping 3C286 in the same way that the H I maps were produced. After all corrections for the GBT efficiency and the mapping process, the scale factor from K/Beam to Jy/Beam images is 0.43 ± 0.03. Due to the patchwork nature of the observations, the RMS noise varies considerably across the datacube, ranging between 6-30 mJy/beam. The average RMS noise in the final data cube is 20 mJy per 24.4 kHz channel. Figure 3 shows the map sensitivity as a function of position. The instrumental parameters are summarized in Table 2, and Table 3 gives a summary of the observations. The spectral line images are available on-line[3].

[2]Developed by the National Radio Astronomy Observatory; documentation at http://gbtidl.sourceforge.net, http://www.aoc.nrao.edu/aips

4. Data Interpretation

In order to detect either H I clouds associated with dark matter minihalos , or cold accretion, a large-area map is required. H I clouds in dark matter minihalos are predicted to be found at distances of up to 1 Mpc from a major halo (Blitz et al. 1999). Cold accretion clouds and interaction-generated clouds are expected to be contained within a $\sim$ 60 kpc radius around large galaxies (Chynoweth et al. 2008; Kereš & Hernquist 2009). Our map has a projected size of 480 kpc × 1.2 Mpc, which is adequate to detect all three phenomena.

Spectral maps were made in the velocity range overlapped by all observations, from -890 to 1320 km s^{-1}. Spectral maps were visually inspected for possible new H I clouds. We required a cloud candidate to be visible in at least two channels, therefore the lowest velocity width that could be detected was 10 km s^{-1} . For each candidate, a plot of intensity versus velocity was also produced and checked. At the locations of strong continuum radio sources, the linear spectral baseline fit was occasionally poor. In these cases, the spectra would show a broad slope, $>$ 400 km s^{-1} wide, either increasing or decreasing with frequency. Candidates in the regions with poor spectral baseline were also discarded. Only 26 of the more than 10,000 GBT beams covering the map showed spectra with poor spectral baselines.

The mass detection threshold was calculated assuming that clouds would be unresolved in the GBT beam, using the relation:

[3] http://www.nrao.edu/astrores/m81/

$$\left(\frac{\sigma_M}{M_\odot}\right) = 2.36\times10^5 \left(\frac{D}{\mathrm{Mpc}}\right)^2 \left(\frac{\sigma_s}{\mathrm{Jy}}\right) \left(\frac{\Delta V}{\mathrm{km\ s^{-1}}}\right) \sqrt{N}, \quad (1)$$

where D is the average distance to the filament, σ_s is the RMS noise in one channel, ΔV is the channel width, and N is the number of channels required for a secure detection. For this calculation, we used an H I cloud linewidth of 20 km s^{-1}, corresponding to $N = 4$. This assumed linewidth strikes a balance between narrower HVC lines (Wakker & van Woerden 1997) and the wider linewidths of massive H I clouds (Chynoweth et al. 2008).

Adopting the M81 distance of 3.6 Mpc, the 1σ mass detection threshold ranges from 2.5 to 12.9 $\times$ 10^5 M$_\odot$, as shown in Figure 3. The average 5σ detection threshold for H I mass was 3.2 $\times$ 10^6 M$_\odot$. With this threshold, we would be able to detect analogues to the most massive clouds around M31 and M33, the M81/M82 clouds, the M101 cloud, and large Milky Way objects such as Complexes C and H and the Magellanic Stream. We would also be able to detect cold accretion clouds found in the simulations of Kereš & Hernquist (2009).

5. New Identifications

We discovered 5 new H I clouds. We divide these clouds into two groups, those associated with the M81 Filament and those associated with the Milky Way. We determine the most likely association of each cloud based on its position and velocity. There is some overlap in velocity space between the M81 Filament and the Milky Way, and over the velocity range -85 to 25 km s^{-1}, we can not discriminate between local and distant emission. In addition, the Galactic HVC Complex A, which ranges in velocity from -120 km s^{-1} to -200 km s^{-1}, coincides with part of the mapped region (Wakker & van Woerden 1997). Therefore we cannot distinguish H I clouds in this position and velocity range from Complex A.

All of the H I clouds we previously detected (Chynoweth et al. 2008, 2009) are visible in this extended image. Their locations are marked in Figure 1. In order to unify the clouds identified in this paper with those in Chynoweth et al. (2008) and Chynoweth et al. (2009), and any H I clouds identified with the GBT in our current and future observations, we have re-designated the clouds with the identifier GBC for "Green Bank Cloud", and the coordinates of the cloud, i. e. GBC Jhhmmss.s+ddmmss. These designations are found in Table 3. To distinguish the newly discovered clouds from the clouds previously discovered, the new clouds are designated with C10-1 to C10-5. Table 3 lists their properties. Spectra are shown in Figure 4. Figure 2 shows the locations of all H I clouds that we have determined to be located within M81 Filament.

Cloud masses were calculated using

$$\left(\frac{M}{M_\odot}\right) = 2.36\times10^5 \left(\frac{D}{\mathrm{Mpc}}\right)^2 \left(\frac{F}{\mathrm{Jy}}\right) \left(\frac{\Delta V}{\mathrm{km\ s^{-1}}}\right), \quad (2)$$

where F is the total flux of the cloud. Error estimates on the masses difficult to obtain, given the wide range in RMS noise values over the map. The dominant error contribution is the approximately 7% uncertainty in the absolute calibration for these observations.

5.1. M81 Filament Clouds

Cloud C10-1 (GBC J092635.8+702850) is to the northwest of the M81 group. With a velocity of -178 km s^{-1}, Cloud C10-1 may be part of Complex A. However, Complex A does not overlap in position with Cloud C10-1, so we include this cloud in further analysis of H I clouds in the M81 Filament.

Cloud C10-2 (GBC J101926.3+675222) is south of IC 2574 and an adjacent HIJASS source, HIJASS J1021+6840 (Boyce et al. 2001) and has a velocity of 38 km s^{-1}. Cloud C10-3 (GBC J091952.7+680937) is to the southwest of the M81 group and has a velocity of -108 km s^{-1}. Cloud C10-4 (GBC J1022:39.1+684057) is located near the previously reported HIJASS source. This cloud is relatively bright and is a few arc-minutes east of the HIJASS source. Boyce et al. (2001) find the HIJASS source is extended in the direction of IC 2574. Our observations have higher angular resolution, and in these observations Cloud C10-4 is clearly separated from HIJASS J1021+6840. Cloud C10-4 has a velocity of 69 km s^{-1}.

5.2. Milky Way Clouds

Cloud C10-5 (GBC J071051.4+654428) is west of the clouds reported in Chynoweth et al. (2009) and shows a high negative velocity. It is visible in 5 channels and is extended spatially. It is offset by about 100 km s^{-1} from Complex A, and may be a separate Milky Way HVC. Cloud C10-5 has a velocity -301 km s^{-1} , which falls outside the velocity range of Complex A (Wakker & van Woerden 1997). There are Galactic HVCs detected with velocities a large as -450 km s^{-1} (Wakker & van Woerden 1991). These observations can not confidently determine whether Cloud 10-5 is associated with the M81 Filament or with the Milky Way.

6. Comparison with Numerical Simulations

In order to determine whether the H I clouds in the M81 Filament have the properties expected for gas-embedded dark-matter halos, we have compared their properties statistically with the properties of dark matter halos generated by N-body simulations. Analysis includes the clouds detected in this paper, in addition to the clouds from Chynoweth et al. (2008) and Chynoweth et al. (2009). For this analysis we only include the H I clouds located in the $8^\circ \times 8^\circ$ region centered on M81, due to the greater RMS noise and contamination by Complex A in other regions of the map. Therefore this analysis excludes clouds C10-5, C09 -1, C09-2, and C09-3. Figure 2 shows the region of the M81 Filament that was compared to the simulation, with H I clouds marked.

We conducted two dark matter-only cosmological N-body simulations for comparison. One simulation uses initial conditions from WMAP3, and one from WMAP5. We simulated a 50^3 Mpc^3 volume of the universe from z=149 to z=0 using 256^3 particles. At redshift zero, we selected a volume 10 Mpc on a side to resimulate with 512^3 particles with a 'zoom' technique aimed to preserve the tidal field outside the higher resolution volume. This smaller volume was selected to host a $\sim 10^{12} M_\odot$ halo at z=0 – this halo is consistent with the M81 galaxy. Figure 5 shows a z=0 snapshot of the simulation. We used a friends-of-friends algorithm with a linking length of $b = 0.2$ to identify dark matter halos, and used a SUBFIND technique to determine the bound subhalos.

In order to connect the numerical simulations with the properties of H I observations, we require an estimate of the H I to dark matter mass fraction. The distribution of H I gas compared to the dark matter halo distribution is very uncertain. For the purpose of comparing our observations with the H I clouds, we assume that H I gas follows the dark matter distribution. We include in our comparison the prescription of Gnedin (2000), which includes a mass cutoff such that a dark matter halo with mass less than 2×10^8 $M_\odot$ has no associated H I gas. We take as the scaling factor from dark matter to H I gas mass the Zwaan et al. (2003) results, summarized in Fukugita & Peebles (2004). Their values yield a H I to dark matter mass fraction of 0.0018 ± 0.0003.

After scaling the simulated dark matter to H I , the WMAP3 simulation contains 7 dark matter halos with a simulated H I mass between 10^{9-10} $M_\odot$, and the WMAP5 simulation contains 8. This is approximately consistent with the M81 H I mass of 2.67×10^9 $M_\odot$. For each of these 'major' halos, we extract a box corresponding to the $8^\circ \times 8^\circ$ region centered on M81. We then apply the 5σ H I mass threshold and velocity limits of our survey.

For each major halo, we find the properties of sub-halos that would be detectable as H I clouds in our observations. We repeat this process rotating the cube three ways. The difference between the expected and observed number of clouds is striking. In the simulation, we find an average of 41 clouds for the WMAP3 simulation and 50 clouds for the WMAP5 simulation (ranging from 12-135 and 16-162 clouds, respectively) per major halo with sufficient mass to be detected in our observations. Recall that 9 clouds were detected in the corresponding region of our observations.

We compare the positions and velocities of the detected clouds with the dark matter halos identified in the simulation, using a 2-dimensional Kolmogorov-Smirnov (KS) test. Figure 6 is a 2-dimensional phase-space diagram showing the distribution of positions and velocities of all observed H I clouds, along with all detectable subhalos, around each major halo, including all rotations, in the simulation. It is clear from the figure that the H I clouds do not fall in the same region as the simulations; the H I clouds are much more concentrated around the central galaxy in both position

and velocity than the dark-matter halos. The results of the 2-dimensional KS-test bear this out, giving an average probability of 8.0 % for WMAP3 and 7.0 % for WMAP5 (across all rotations of all major halos) that the position-velocity distributions are consistent.

7. Discussion, Conclusions and Future Work

We observed a wide area of the nearby M81 filament in an attempt to find H I clouds tracing dark matter minihalos predicted by ΛCDM cosmological simulations. We detected 5 new H I clouds, bringing the total to 13 H I clouds in the M81 Filament including our previously published observations.

Of the 13 clouds detected in the observed region, 4 are likely to be part of the Milky Way HVC system. We compared the properties of the remaining 9 H I clouds to two cosmological dark matter N-body simulations. We find that there are far fewer H I clouds than simulations predict, and that the phase space distribution of the detected H I clouds does not match that of the simulated clouds. There are two possible explanations for this discrepancy, both of which may be true. First, the H I to dark matter mass fraction in minihalos may be less than 0.18%. Secondly, the phase space distribution of dark matter minihalos predicted by ΛCDM cosmological simulations may be incorrect.

Because our simulations are dark-matter only, none of the simulated clouds are tidal debris (which would contain no dark matter). With these simulations, we cannot predict the properties of H I clouds representative of tidal debris, but we can confidently say that the clouds we have detected do NOT match the properties expected for dark-matter minihalos. The detected H I clouds are also not compatible with cold accretion, since we do not detect clouds near non-interacting galaxies– cold accretion clouds should be detectable regardless of interactions. In fact, recent research suggests that cold accretion clouds should be *more* prevalent in non-interacting groups, due to the lack of mitigating environmental effects (Oosterloo et al. 2010).

Therefore, we conclude that the H I clouds we have detected are not likely to be tracers of the predicted dark-matter minihalos in the M81 Filament. Instead, they are most likely generated through galaxy interactions. In order to understand the detailed role of galaxy interactions in generating H I clouds, further simulations including gas physics and deeper observations of more filaments are needed.

This study allows us to constrain the number of detected H I clouds that may be self-gravitating. In a study of gravitationally bound molecular clouds, Larson (1979, 1981) found a strong correlation between velocity dispersion and cloud size, given by

$$\sigma_v(\text{km s}^{-1}) = 1.1\ \text{L(pc)}^{0.38}, \tag{3}$$

where L is the diameter of the cloud. Our survey detection threshold of $\sigma_v = 10$ km s^{-1} gives a cloud size of 330 pc, so the angular resolution of our observations (10 kpc) is the limiting factor in detecting self-gravitating H I clouds. All of our clouds are unresolved in the GBT beam. Our angular resolution limit gives a velocity dispersion of 36 km s^{-1}, so for any of the detected clouds to be self-gravitating they must have a velocity dispersion less than or equal to this value. Only two of the 9 clouds that we have determined to reside in the M81 group satisfy this constraint. The implication of this constraint is that most interaction-generated H I clouds in our detection space are not self-gravitating.

On a side note, dark-matter filaments such as the M81 Filament are predicted to have diffuse H I emission (Popping et al. 2009). The emission is predicted to be approximately 3 times fainter than our survey. Our observations do, however, place an upper limit on diffuse H I emission from the cosmic web.

To estimate this, we determined our column density sensitivity using:

$$\left(\frac{\sigma_{N_{HI}}}{N_{HI}}\right) = 1.82 \times 10^{18} \left(\frac{\sigma_{T_B}}{K}\right) \left(\frac{\Delta V}{\text{km s}^{-1}}\right) \sqrt{N} \tag{4}$$

The average 5σ detection threshold for H I column density was 4.4×10^{18} cm^{-2}. This column density falls within the "H I Desert", where the gas in the cosmic web is not affected by self-shielding and is therefore photoionized (Popping et al. 2009). Hence, we did not expect to detect

diffuse H I in the filament between the two galaxy groups. Our lowest 5σ detection threshold for H I column density was $\sim 1 \times 10^{18}$ cm^{-2}, which is approximately 3 times too high to detect the diffuse cosmic web in H I emission. More sensitive GBT and EVLA observations of smaller regions, or surveys by future radio telescopes, could reach the sensitivity required to detect this emission.

KMC thanks the NRC Research Associateship program, the NRAO Pre-Doctoral Fellowship program, and Vanderbilt University for funding support. *Facilities:* GBT.

REFERENCES

Begum, A., Chengalur, J. N., Karachentsev, I. D., Kaisin, S. S., & Sharina, M. E. 2006, MNRAS, 365, 1220. arXiv:astro-ph/0511253

Blitz, L., Spergel, D. N., Teuben, P. J., Hartmann, D., & Burton, W. B. 1999, ApJ, 514, 818. arXiv:astro-ph/9803251

Boyce, P. J., Minchin, R. F., Kilborn, V. A., Disney, M. J., Lang, R. H., Jordan, C. A., Grossi, M., Lyne, A. G., Cohen, R. J., Morison, I. M., & Phillipps, S. 2001, ApJ, 560, L127. arXiv:astro-ph/0109086

Braun, R., & Burton, W. B. 1999, A&A, 341, 437. arXiv:astro-ph/9810433

Bregman, J. N. 1980, ApJ, 236, 577

Chynoweth, K. M., Langston, G. I., Holley-Bockelmann, K., & Lockman, F. J. 2009, AJ, 138, 287. 0905.0906

Chynoweth, K. M., Langston, G. I., Yun, M. S., Lockman, F. J., Rubin, K. H. R., & Scoles, S. A. 2008, AJ, 135, 1983. arXiv:0803.3631

Dekel, A., & Silk, J. 1986, ApJ, 303, 39

Fukugita, M., & Peebles, P. J. E. 2004, ApJ, 616, 643. arXiv:astro-ph/0406095

Giovanelli, R., Haynes, M. P., Kent, B. R., & Adams, E. A. K. 2010, ApJ, 708, L22. 0911.4195

Gnedin, N. Y. 2000, ApJ, 542, 535. arXiv:astro-ph/0002151

Karachentsev, I. D., Dolphin, A. E., Geisler, D., Grebel, E. K., Guhathakurta, P., Hodge, P. W., Karachentseva, V. E., Sarajedini, A., Seitzer, P., & Sharina, M. E. 2002, A&A, 383, 125

Karachentsev, I. D., & Kaisin, S. S. 2007, AJ, 133, 1883. arXiv:astro-ph/0701465

Kereš, D., & Hernquist, L. 2009, ApJ, 700, L1. 0905.2186

Klypin, A., Kravtsov, A. V., Valenzuela, O., & Prada, F. 1999, ApJ, 522, 82. arXiv:astro-ph/9901240

Kravtsov, A. V., Gnedin, O. Y., & Klypin, A. A. 2004, ApJ, 609, 482. arXiv:astro-ph/0401088

Langston, G., & Turner, B. 2007, ApJ, 658, 455

Larson, R. B. 1979, MNRAS, 186, 479

— 1981, MNRAS, 194, 809

Oosterloo, T., Morganti, R., Crocker, A., Jütte, E., Cappellari, M., de Zeeuw, T., Krajnović, D., McDermid, R., Kuntschner, H., Sarzi, M., & Weijmans, A. 2010, MNRAS, 1397. 1007.2059

Ott, M., Witzel, A., Quirrenbach, A., Krichbaum, T. P., Standke, K. J., Schalinski, C. J., & Hummel, C. A. 1994, A&A, 284, 331

Pisano, D. J., Barnes, D. G., Gibson, B. K., Staveley-Smith, L., Freeman, K. C., & Kilborn, V. A. 2007, ApJ, 662, 959. arXiv:astro-ph/0703279

Popping, A., Davé, R., Braun, R., & Oppenheimer, B. D. 2009, A&A, 504, 15. 0906.3067

Putman, M. E., & Moore, B. 2002, in Extragalactic Gas at Low Redshift, edited by J. S. Mulchaey & J. T. Stocke, vol. 254 of Astronomical Society of the Pacific Conference Series, 245. arXiv:astro-ph/0110417

Putman, M. E., Staveley-Smith, L., Freeman, K. C., Gibson, B. K., & Barnes, D. G. 2003, ApJ, 586, 170. arXiv:astro-ph/0209127

Ricotti, M. 2009, MNRAS, 392, L45. 0806.2402

Thilker, D. A., Braun, R., Walterbos, R. A. M., Corbelli, E., Lockman, F. J., Murphy, E., & Maddalena, R. 2004, ApJ, 601, L39. arXiv:astro-ph/0311571

Wakker, B. P., & van Woerden, H. 1991, A&A, 250, 509

— 1997, ARA&A, 35, 217

Zwaan, M. A., Staveley-Smith, L., Koribalski, B. S., Henning, P. A., Kilborn, V. A., Ryder, S. D., Barnes, D. G., Bhathal, R., Boyce, P. J., de Blok, W. J. G., Disney, M. J., Drinkwater, M. J., Ekers, R. D., Freeman, K. C., Gibson, B. K., Green, A. J., Haynes, R. F., Jerjen, H., Juraszek, S., Kesteven, M. J., Knezek, P. M., Kraan-Korteweg, R. C., Mader, S., Marquarding, M., Meyer, M., Minchin, R. F., Mould, J. R., O'Brien, J., Oosterloo, T., Price, R. M., Putman, M. E., Ryan-Weber, E., Sadler, E. M., Schröder, A., Stewart, I. M., Stootman, F., Warren, B., Waugh, M., Webster, R. L., & Wright, A. E. 2003, AJ, 125, 2842. arXiv: astro-ph/0302440

Appendix A: Properties of Known Galaxies

Our survey encompasses a large volume and we have detected a significant number of galaxies in H I . We calculated H I masses of all known galaxies in the observed volume using:

$$\left(\frac{M}{M_\odot}\right) = 2.36 \times 10^5 \left(\frac{D}{\mathrm{Mpc}}\right)^2 \left(\frac{F}{\mathrm{Jy}}\right) \left(\frac{\Delta V}{\mathrm{km\ s^{-1}}}\right) \quad (5)$$

Where F is the total flux of the galaxy.

Distances for galaxies in the M81 Filament were taken from Karachentsev & Kaisin (2007). Distances to background galaxies were taken from NED where available; otherwise, they were calculated from the radial velocity, assuming a Hubble constant of $H_0 = 75$ km s^{-1} Mpc^{-1}. Because of the high number of galaxies and continuum sources in the field, each galaxy spectrum was rebaselined using a first-order fit to the surrounding spectral region, in order to calculate an accurate H I mass.

This 2-column preprint was prepared with the AAS LaTeX macros v5.2.

Table 1: Parameters of the Robert C. Byrd Green Bank Telescope System

Telescope:	
Diameter.....	100 m
Beamwidth (FWHM).....	9.1 $'$
Linear resolution	2.7 D_{Mpc} kpc
Receiver:	
Typical System Temperature	20 K
Spectrometer:	
Bandwidth.....	12.5-50 MHz
Resolution, Hanning Smoothed.....	6.1 kHz (1.29 km s^{-1})

Table 2: Observations Summary

Center Frequency (MHz)	1419.4
Bandwidth (MHz)	10.5
Channel Width (kHz)	24.4
Velocity Resolution (km s^{-1})	5.2
Integration time (hours):	187
Typical RMS noise (mJy)	20
Sensitivity to H I (5σ)	3.2 $\times$ 10^6 M$_\odot$

Table 3: M81 Filament H I Cloud Properties[a]

Cloud [b]	Coordinate Designation	ΔD$_{M81}$ (kpc)	T$_{peak}$ (K)	V$_{LSR}$ (km s^{-1})	σ_v (km s^{-1})	M$_{HI}$ $(\frac{D}{3.63Mpc})^{-2}$ $\times$ 10^{6}M$_\odot$
C08-1	GBC J095007.2+695556	65	0.11	168	50	14.7
C08-2	GBC J100250.7+681949	63	0.10	-102	55	22.5
C08-3	GBC J095244.9+681250	57	0.12	14	82	26.7
C08-4	GBC J100145.0+691631	38	0.30	74	28	83.7
C08-5	GBC J095506.3+692205	21	0.07	283	36	6.9
C09-1	GBC J073236.0+654302	900	0.06	-147	20	1.8
C09-2	GBC J072528.5+654922	937	0.15	-113	20	7.5
C09-3	GBC J073612.1+673325	826	1.97	-202	30	62.6
C10-1	GBC J092635.8+702850	186	0.13	-178	57	3.6
C10-2	GBC J101926.3+675222	161	0.20	38	26	3.4
C10-3	GBC J091952.7+680937	218	0.17	-108	42	5.1
C10-4	GBC J1022:39.1+684057	159	0.30	69	68	12.0
C10-5	GBC J071051.4+654428	1024	0.19	-301	47	2.8

[a] Includes clouds discovered in Chynoweth et al. (2008) and Chynoweth et al. (2009).

[b] C08 indicates clouds from Chynoweth et al. (2008), C09 indicates clouds from Chynoweth et al. (2009), and C10 indicates clouds that are new in this paper.

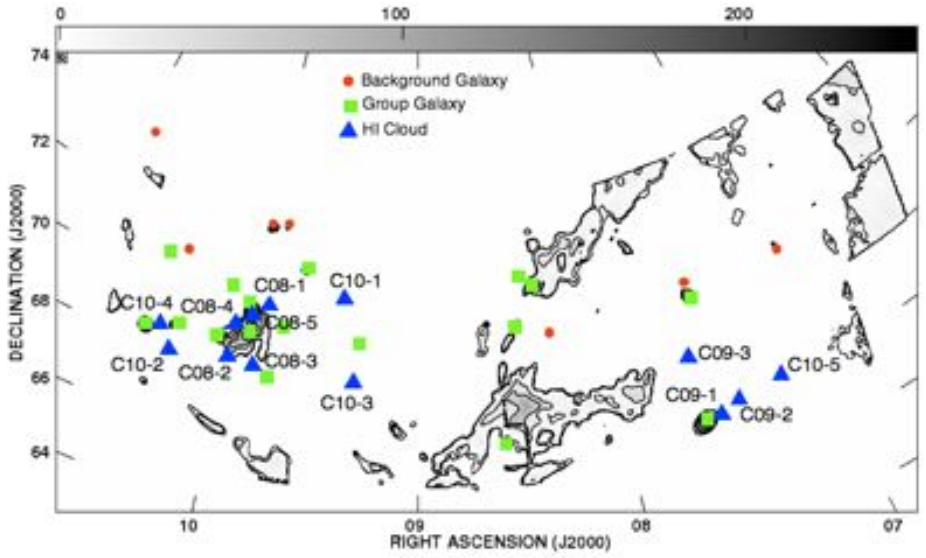

Fig. 1.— H I column density map of the observed area. Background galaxies, group galaxies, and H I clouds are marked. The diagonal filament of H I through the middle of the map is Milky Way HVC Complex A.

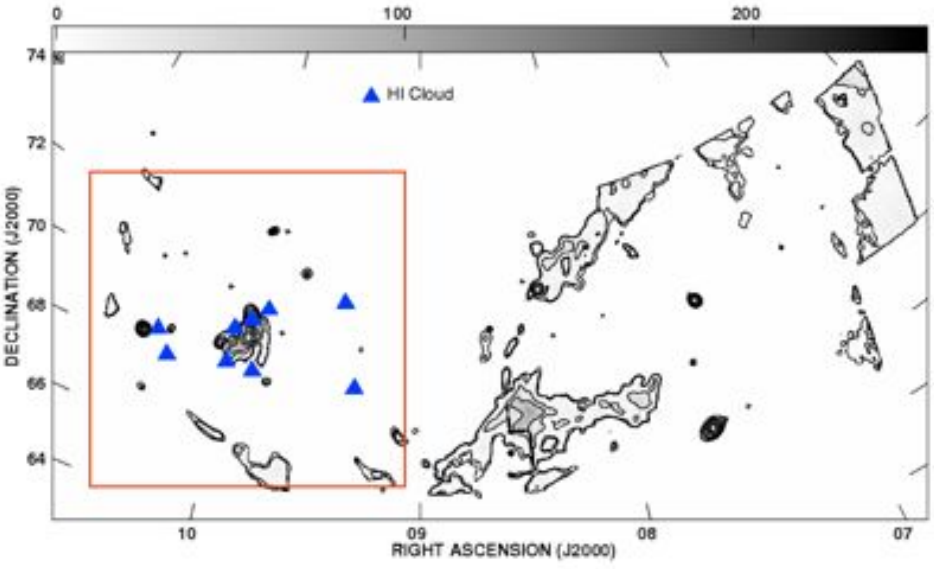

Fig. 2.— H I clouds that are located within the M81 Filament are labeled with triangles.The region of the M81 Filament that was compared to a cosmological dark-matter simulation is indicated with a red box.

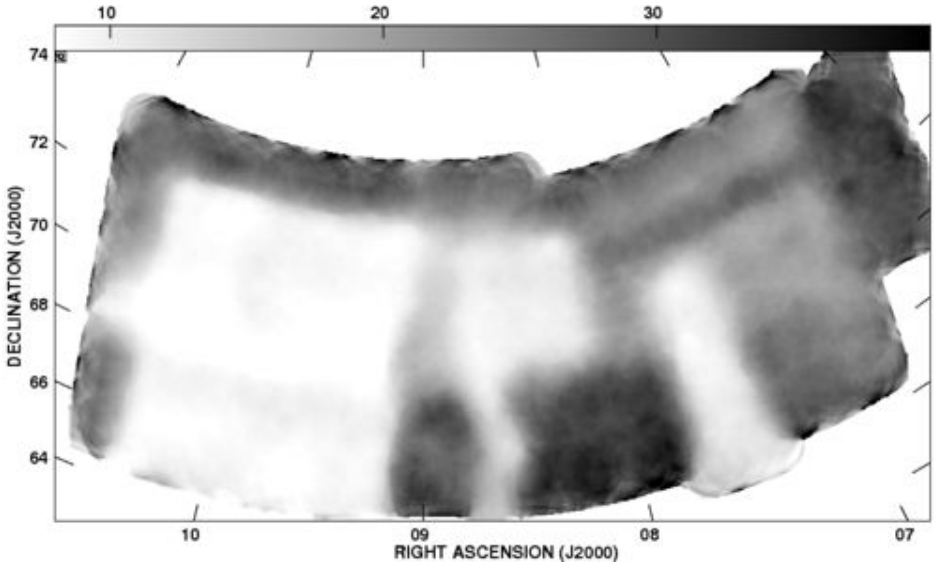

Fig. 3.— Sensitivity of the mapped area. The greyscale ranges from 8 to 40 mJy beam^{-1}, corresponding to mass sensitivity of 2.5 to 12.9 $\times$ 10^5 $M_\odot$. The colorbar above the figure is in units of mJy beam^{-1}.

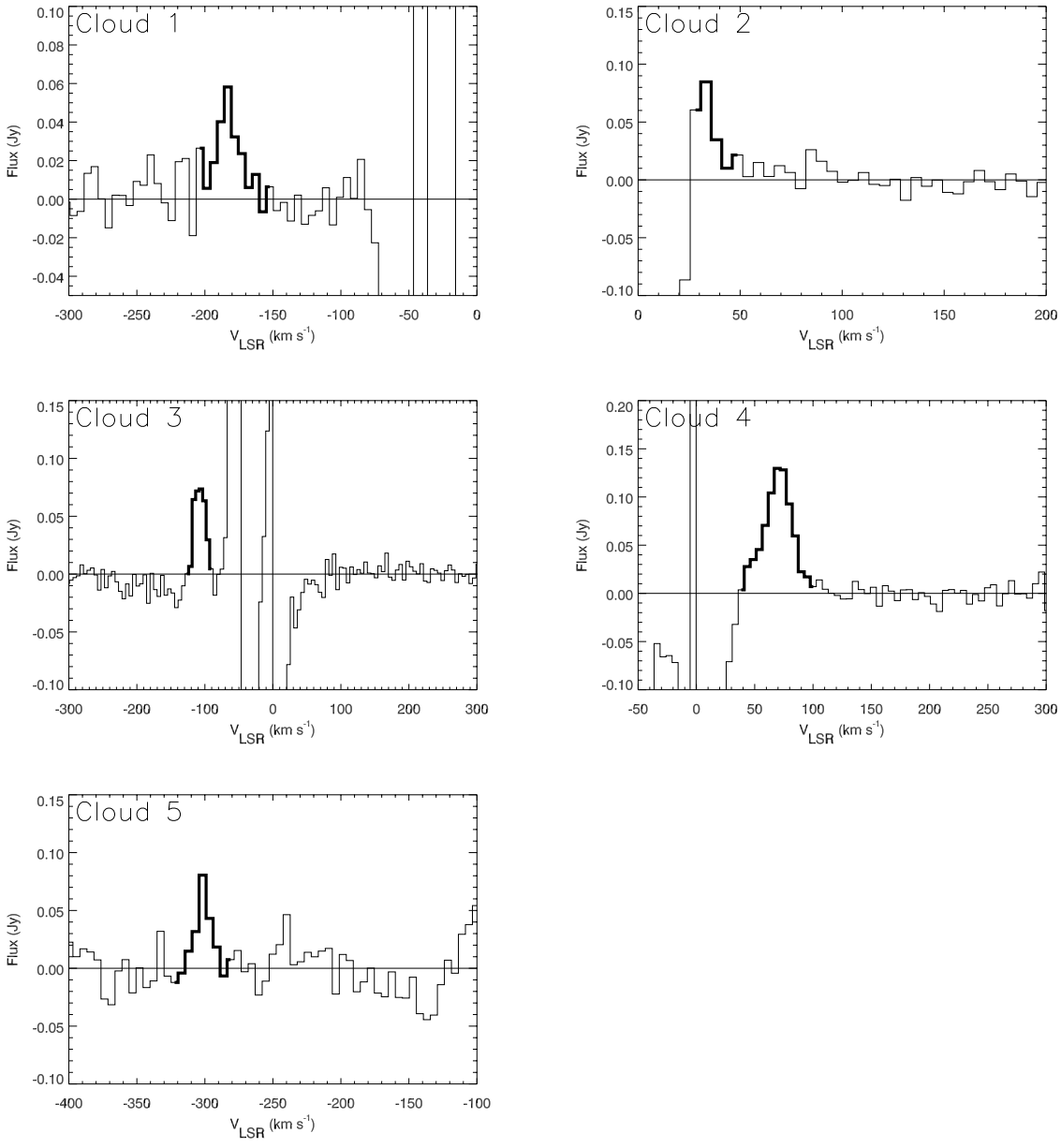

Fig. 4.— H I intensity profiles of new H I clouds. The regions of the spectrum used to calculate H I mass are highlighted in bold.

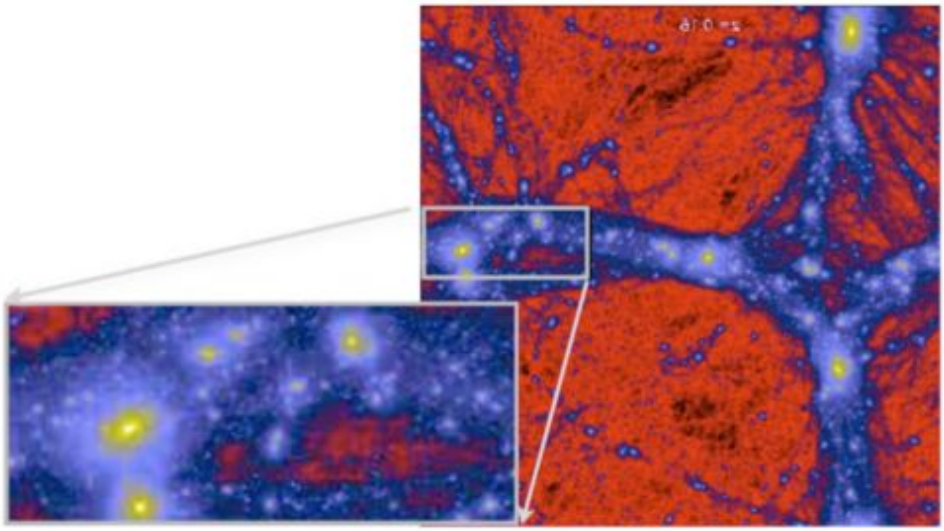

Fig. 5.— Snapshot of the projected density of dark matter in the cosmological simulation used to find expected properties of halos. The large box is 10 Mpc on a side. The highlighted box corresponds to the angular size of our observations.

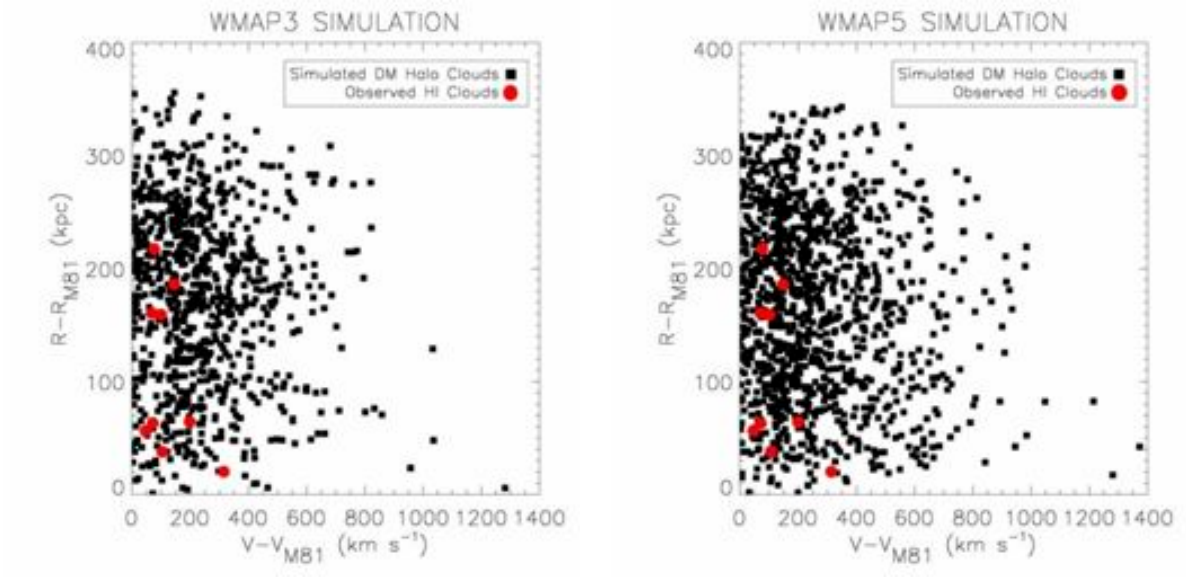

Fig. 6.— Comparison of positions and velocites of H I clouds in the 8° × 8° region centered on M81 with the expected properties of dark-matter halos with a 0.18% H I /total mass fraction. Left: Simulation with WMAP3 parameters. Right: Simulation with WMAP5 parameters. All detectable minihalos from each rotation of each major halo in the simulation are plotted. Note that the H I clouds are much more clustered in position and velocity than dark-matter halos.

Table 4: Properties of Known Galaxies[a]

Name	α^{b} (J2000)	δ^{b} (J2000)	D[c] Mpc	V_{LSR}[d] km s^{-1}	M_{HI} $\times 10^{9} M_{\odot}$
UGC 3580	06:55:30.8	69:33:47	15.90	1193	2.59
NGC 2366	07:28:55.7	69:12:59	3.19	102	0.68
KUG 0724+695	07:29:50.0	69:25:26	12.02	902	0.27
NGC 2403	07:36:52.7	65:35:52	3.30	134	3.38
KKH 44	08:16:38.5	69:20:49	14.08	1056	0.06
UGC 4305	08:19:06.5	70:43:01	3.39	160	0.91
KDG 52	08:23:56.2	71:01:36	3.55	116	0.02
DDO 53	08:34:08.6	66:11:03	3.56	23	0.05
UGC 4483	08:37:03.1	69:46:44	3.21	159	0.04
NGC 2787	09:19:18.5	69:12:12	9.31	716	0.72
Holmberg I	09:40:32.3	71:10:56	3.84	152	0.16
BK1N	09:45:15.3	69:23:22	7.86	584	0.06
NGC 2976	09:47:15.6	67:54:49	3.56	6	0.52
NGC 2985	09:50:22.2	72:16:43	16.45	1213	3.17
NGC 3027	09:55:40.6	72:12:13	14.12	1061	4.74
M81	09:55:33.5	69:03:60	3.63	-32	2.67
M82	09:55:53.9	69:40:57	3.53	206	0.75
NGC 3077	10:03:21.0	68:44:02	3.82	17	1.01
UGC 5423	10:05:30.6	70:21:52	5.30	350	0.03
HIJASS J1021+68	10:20:30.1	68:39:25	3.70	64	0.08
UGC 5612	10:24:06.5	70:52:56	13.67	1025	0.98
IC 2574	10:29:19.0	68:27:42	4.02	79	1.36
UGC 5692	10:30:35.0	70:37:07	4.00	69	0.006
NGC 3403	10:53:54.8	73:41:25	15.35	1216	1.84

[a] Values for M81 and NGC 2403 group galaxies are taken from Chynoweth et al. (2008) and Chynoweth et al. (2009).
[b] From NED
[c] From Karachentsev & Kaisin (2007), or cz/HO for D$\geq$ 7 Mpc
[d] From our observations

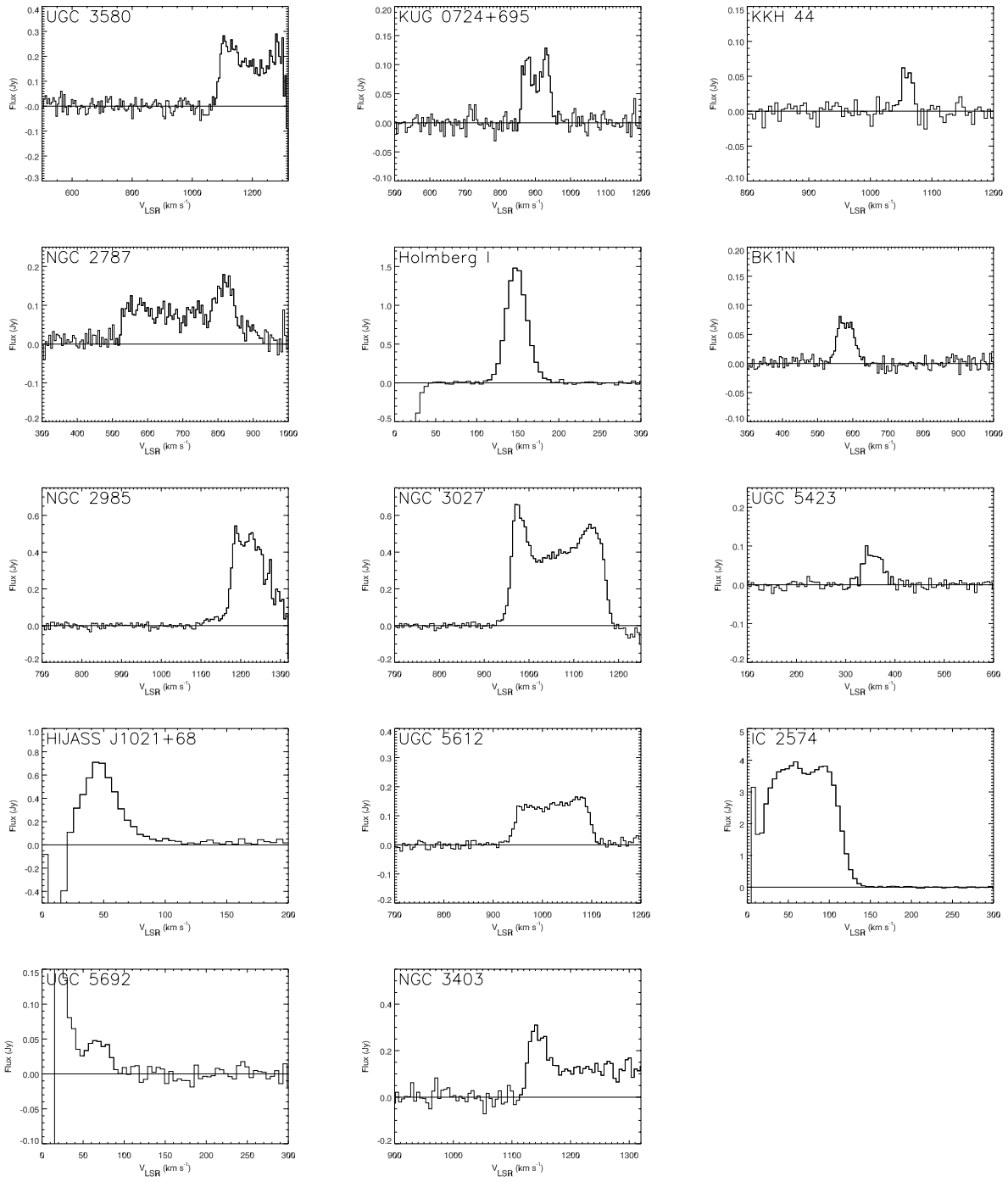

Fig. 7.— H I line profiles of known galaxies within our observed field. Note that some galaxies do not fall completely within our bandwidth, so the derived mass will be low. Line profiles for the galaxies in the M81 and NGC 2403 groups can be found in Chynoweth et al. (2008) and Chynoweth et al. (2009).